Boletín Geológico

SERVICIO GEOLÓGICO COLOMBIANO

Boletín Geológico, 50(1), 2023

https://doi.org/10.32685/0120-1425/bol.geol.50.1.2023.664

Received: May 16, 2022

Revision received: November 18, 2022

Accepted: December 5, 2022

Published online: March, 29, 2023

Review article

Potential of metallogenic fertility of the Triassic-Jurassic magmatism in the Santander Massif, Colombia: A zircon chemistry approach

Potencial de fertilidad metalogénica del magmatismo triásico-jurásico del Macizo de Santander, Colombia: abordaje desde la química del circón

Ana María **Correa Martínez**[1], Gabriel **Rodríguez García**[1]

1. Servicio Geológico Colombiano, Special Geological Studies Group, Medellín, Colombia.
Corresponding author: Ana María Correa Martínez, anmcorreama@unal.edu.co

Abstract

This study uses the trace-elements composition of zircons from various units, generated during the Late Triassic-Jurassic magmatism of the Santander Massif, to infer the metallogenetic fertility potential of Cu (±Mo±Au) in the base metals of the magmas. The evaluation is based on the degree of hydration and the oxidation state since these factors can make the magma fertile for mineralization. The application of fertility indicators, tested by other authors from various Cu (±Mo±Au) porphyry deposits around the world, allows us to conclude that most of the units studied offer fertility potential for Cu (±Mo±Au) base metal deposits. The geological units with the greatest potential for relative fertility are the dioritic facies from La Corcova Monzogranite and from the Páramo Rico Tonalite and Granodiorite. The samples with an intermediate potential are, in decreasing order, those of the Mogotes Batholith, the Rionegro Monzogranite, the Intrusive-Extrusive Igneous Complex and a small amount in the Santa Bárbara Monzogranite. The samples with a possible low potential are the San Joaquín Rhyolite and the Alto Los Cacaos Rhyolites. The San Martín Tonalite has very little or no potential.

Keywords: zircon as a mineral indicator, magma fertility, Cu (±Mo±Au) mineral deposits, granitoids.

Resumen

En este estudio se usan los elementos traza de los circones de varias unidades del magmatismo del límite triásico-jurásico del Macizo de Santander, con el fin de inferir el potencial de fertilidad metalogenética en metales base de Cu (±Mo ±Au) de los magmas. La evaluación se basa en el grado de hidratación y el estado de oxidación como factores que pueden hacer al magma fértil para mineralizaciones. La aplicación de indicadores de fertilidad, probados por otros autores en diversos yacimientos de pórfidos de

Citation: Correa Martínez, A. M., & Rodríguez, G. (2023). Potential of metallogenic fertility of the Triassic-Jurassic magmatism in the Santander Massif, Colombia: A zircon chemistry approach. *Boletín Geológico, 50*(1). https://doi.org/10.32685/0120-1425/bol.geol.50.1.2023.664

Cu (±Mo ±Au) de todo el mundo, permite concluir que la mayoría de las unidades estudiadas presentan potencial fertilidad para los yacimientos de metales base de Cu (±Mo±Au). Las unidades geológicas con mayor potencial de fertilidad relativa son las facies dioríticas de La Corcova y la Tonalita y Granodiorita del Páramo Rico. En orden decreciente, con un potencial intermedio están las del Batolito de Mogotes, el Monzogranito de Rionegro, el Complejo Ígneo Intrusivo-Extrusivo y un cuerpo menor del Monzogranito de Santa Bárbara, mientras que con un posible bajo potencial están la Riolita de San Joaquín y las Riolitas del Alto Los Cacaos. Con muy bajo o nulo potencial se encuentra la Tonalita de San Martín.

Palabras clave: circón como indicador mineral, fertilidad del magma, depósitos minerales de Cu (±Mo ±Au), granitoides.

1. Introduction

The igneous suite at the Late Triassic-Early Jurassic boundary in the Santander Massif (Colombian Andes), which are known as the Santander Plutonic Group (Ward et al., 1973), has been the subject of several petrogenetic studies (Goldsmith et al., 1971; Ward et al., 1973; Restrepo-Pace, 1995; Restrepo-Pace et al., 1997; Ordóñez-Carmona, 2001; van der Lelij et al., 2016, 2019; Rodríguez et al., 2017; Leal-Mejía et al., 2019; López-Isaza and Zuluaga, 2020; Rodríguez et al., 2020a, 2020b). However, little research has been done that relates to the potential metallic mineral deposits within those units (Mantilla Figueroa et al., 2001; Mantilla and Mesa, 2002; Gamboa Herrera, 2016; Prieto et al., 2019). No significant mineralizations of Cu, Pb, Zn, Mo, W, Sn and ±Au associated with this magmatism have been discovered. However, the existence of type I and type S granites, both peraluminous and metalluminous (van der Lelij et al., 2016; Zuluaga and López, 2019; Rodríguez et al., 2020a, 2020b), suggests different formation conditions for these granites and reveals the possibility of various mineral deposits.

Traditionally, the analysis of the metallogenetic fertility potential of magmas has been carried out with indicators based on total rock geochemistry (Blevin and Chappell, 1992, 1995; Chiaradia et al., 2012; Loucks, 2014; Richards, 2015; Cheng et al., 2018). However, this type of study has limitations due to the mobility driven by hydrothermal alteration or weathering of some present chemical elements (Lu et al., 2016). In recent years, studies on potential mineral fertility have been based on the composition of trace elements, namely zircon, as it is a mineral resistant to subsolidus modifications, which can preserve the compositional characteristics of magmas that form metallic mineral deposits (Ballard et al., 2002; Belousova et al., 2006; Rohrlach and Loucks, 2005; Lu et al., 2016). The composition of zircon, especially its trace elements, reflects the redox states of magma (Ballard et al., 2002; Hoskin and Schaltegger, 2003; Burnham and Berry, 2012; Dilles et al., 2015; Shen et al., 2015) and serves as an indicator of porphyry-type Cu-Au-(Mo) deposits (Dilles et al., 2015; Lu et al., 2016, 2019; Cooke et al., 2017), Sn-W mineralization in granitoids (Gardiner et al., 2017) and Cu-Pb-Zn skarn deposits (Zhong et al., 2018).

This article presents the reinterpretation of the trace element compositions of zircons from various igneous units belonging to the Triassic-Jurassic boundary of the Santander Massif (Rodríguez et al., 2017; 2020c, 2020d, 2020e, 2020f; Correa Martínez et al., 2020a, 2020b; Arango et al., 2020). The purpose of this reinterpretation was to analyze the metallogenetic fertility potential of Cu (±Mo±Au) in the granitoid-forming magmas. The information obtained from the zircon serves as a mineral exploration tool to predict possible exploration targets in geological units of the Santander Massif.

2. Background on the metallogenetic fertility potential of magma

The metallogenetic fertility of a magma refers to its predisposition to form magmatic-hydrothermal mineral deposits of precious metals and bases, which depends on the capacity of the magmatic system to exsolve vapors and metal-rich fluids (Cooke et al., 2009; Sillitoe, 2010). The main parameters that determine the metallogenetic fertility potential of igneous suites relate to the tectonic environment, the type of rock, the source and compositional evolution, the degree of fractionation and the hydration and oxidation states of the granitoid-forming magmas (Ishihara, 1981; Blevin and Chappell, 1992; Richards et al., 2012; Gardiner et al., 2017).

In general, magmas resulting from melting of igneous protoliths in the crust tend to be more oxidized (forming granites of the magnetite series), and they produce I-type granites. Their associated mineral deposits often have significant concentrations of Cu, Pb, Zn, Mo, and Au. On the other hand, the

magmas derived from partial melting of sedimentary or supracrustal rocks are more felsic, reduced (derived from granites belonging to the ilmenite series), and generate S-type granites that contain mineral deposits characterized by the presence of Sn, W, U and Th (Chappell and White, 1974; Ishihara, 1978, 1981; Robb, 2005).

Specifically, Cu (-Au) deposits are associated with the more mafic end of the granitoid spectrum, which derives from oxidized, relatively unevolved, moderately fractionated, and hydrated magmas (Belvin and Chappell, 1995; Sillitoe, 2010). Mo is related to fractionated felsic granites and oxidized magmas, while W is related to magmas of intermediate compositions and with intermediate to relatively low oxidation states (Blevin and Chappell, 1992, 1995). W-Mo deposits are formed in granitic magmas with intermediate fractionation (Blevin et al., 1996; Thompson et al., 1999; Cheng et al., 2018). Tin deposits are associated with highly fractionated felsic granites and reduced magmas. Skarn deposits are similar in many aspects of their origin and evolution to those of the porphyry-type (Sillitoe, 2010; Zhong et al., 2017).

Magmas that form mineral deposits have distinctive whole-rock geochemical and trace-element compositions of zircons relative to nonmineralized magmas (Lu et al., 2016). These compositions can be indicators of fertility, and in the case of Cu porphyry systems related to arc magmas, they are explained by high magmatic sulfur and water contents that generate high oxidation and hydration states; therefore, they favor the transport and precipitation of metals (Ballard et al., 2002; Richards et al., 2012; Chiaradia et al., 2012; Loucks, 2014).

Zircon is used as an indicator of the potential fertility of magma (Ballard et al., 2002; Richards et al., 2012; Dilles et al., 2015; Lu et al., 2016; Gardiner et al., 2017). Patterns of rare earth elements (REEs) of typical igneous zircon, normalized to chondrite, exhibit positive Ce and negative Eu anomalies (Hoskin and Schaltegger, 2003). The magnitude of these anomalies varies as a function of the oxygen fugacity (fO_2) of the melt (Ballard et al., 2002; Burnham and Berry, 2012; Trail et al., 2012). The zircons of more oxidized magmatic systems, which in turn are interpreted as more fertile in terms of porphyry-type Cu mineral deposits, exhibit greater positive Ce anomalies and very slight or nonexistent negative Eu anomalies (Ballard et al., 2002; Richards et al., 2012; Chelle-Michou et al., 2014; Dilles et al., 2015; Lu et al., 2016). These authors and others attribute the weak Eu anomaly, in addition to the oxidation state of magma, to the suppression of plagioclase crystallization (a mineral that normally incorporates more Eu^{2+} in its structure than the other of REEs and causes the negative Eu anomaly strength in zircon) in hydrated magmas.

Alternatively, Loader et al. (2017) suggest that weak negative Eu anomalies are dependent on REE concentrations in the melt and not necessarily on redox conditions. The weak negative Eu anomaly can also be explained by the prior or simultaneous crystallization of titanite with zircon, which produces an increase in the Eu/Eu* ratio and a decrease in the negative Eu anomaly within the zircon. In any case, the authors concluded that the Eu anomaly in the zircon, despite being an empirical criterion of the redox conditions of the system, works well as a screening tool to establish the potential for magmatic fertility. In addition, the presence of titanite is also an indicator of fertility.

There are equations proposed by different authors that can approximate the Ce^{4+}/Ce^{3+} relationship and the Ce anomaly, such as those from Ballard et al. (2002) and Loader et al. (2017), or that can approximate the relationships used as proof of enrichment or impoverishment in Ce, such as, for example, the Ce/Nd relationship presented in Chelle-Michou et al. (2014). Loader et al. (2017) argue that the Ce anomaly (Ce/Ce*), although it is a good test of the oxidation conditions, is a semi-quantitative measure of these conditions due to the analytical difficulties in directly quantifying the chemical elements used when calculating the Ce^{4+}/Ce^{3+} and Ce/Ce* relationships (see explanations in Lu et al., 2016, 2017).

According to Lu et al. (2016), the best indicators for the fertile magmatic units in Cu (±Mo±Au) and Mo porphyry-type mineralizations are the values of the relationships Eu/Eu* and 10 000* (Eu/Eu*)/Y, whereas the relationships (Ce/Nd)/Y and Dy/Yb are moderately useful. The Eu/Eu* (> 0.3) and 10 000* (Eu/Eu*)/Y (> 1) ratios indicate high magmatic water contents. The (Eu/Eu*)/Y relationship is consistent with the early fractionation of amphibole that impoverishes Y within the melt, which is a complementary process to the suppression of the early crystallization of plagioclase due to the presence of water in the magma. The Ce/Nd ratio is used as an estimate of the Ce anomaly. The Dy/Yb ratio is proof of the fractionation of amphibole due to the incorporation of middle REEs (MREEs), which is where the fractionation of amphibole within hydrated melts leads to a decrease in the Dy/Yb ratio (Davidson et al., 2007).

Ballard et al. (2002) found that the zircons associated with porphyry-type copper mineralizations in the Chuquicamata-El Abra belt in Chile have Ce^{4+}/Ce^{3+} ratios > 300 and Eu/Eu*> 0.4. In porphyry and epithermal deposits from Chile, Peru

and Nevada, Dilles et al. (2015) observed that Eu/Eu* ratios > 0.4 characterize mineralization-forming intrusions. Lu et al. (2016) found that the fertile magmatic units in porphyry-type Cu-Au-Mo mineralizations have higher Eu/Eu* ratios (> 0.3), 10 000* (Eu/Eu*)/Y (> 1), (Ce/Nd)/Y (> 0.01) and lower ratios of Dy / Yb (<0.3) than within infertile units and exhibit Ce/Nd relationships between approximately 2-110. Loader et al. (2017) and Lu et al. (2019) consider the value of Eu/Eu* ratios > 0.4 as a reference for fertile units.

Gardiner et al. (2017) found that for zircons from arc Cu deposits, the average values of Ce/Ce* vary from 46-350, and for Eu anomalies between 0.19 and 0.24, while for Sn deposits, the average values are, in general, lower and vary between 0.8 and 43, and the Eu/Eu* ratios present values of ca. ≤0.08. These authors calculated the Ce anomaly as follows: $Ce/Ce^* = Ce/(The' Pr)^{0.5}$. Additionally, in zircons with La below the detection limit, they extrapolated a value for Ce* from Pr and Nd on a logarithmic scale.

For *skarn*-type deposits of Cu-Pb-Zn, Zhong et al. (2018) found that fertile intrusions exhibit Ce^{4+}/Ce^{3+} values > 12 and Eu/Eu* values between 0.07 and 0.31. These authors calculated Ce^{4+}/Ce^{3+} by applying the method proposed in Ballard et al. (2002).

As explained by Blevin and Chappell (1992), not all granitoids with fertility potential are mineralized. In addition to causes such as nonexposure or the removal of the preexisting mineralization by erosion, there are other factors that can decisively impact mineralization. Among these are the timing of the liberation of the magmatic aqueous phase as that relates to the degree of crystallization of the pluton and the chemical and structural nature of the wallrocks.

3. Geological context

The study area is located in the Santander Massif in the Eastern Cordillera of the Colombian Andes (Figure 1). This massif consists mainly of a Precambrian and Ordovician metamorphic basement and, to a lesser extent, an igneous basement also Ordovician (Ward et al., 1973; Restrepo-Pace et al., 1997; Cordani et al., 2005; van der Lelij et al., 2016; Rodríguez et al., 2020a; Mantilla Figueroa et al., 2012, 2016; Rodríguez, 2022). Devonian and Carboniferous-Permian sedimentary rocks discordantly cover the basement (Cediel, 1969; Ward et al., 1973). An extensive magmatic event that occurred between the Late Triassic and the Early Jurassic intruded into the basement. Magmatism was followed by volcanism and intracontinental sedimentation between the Early and Late Jurassic (Ward et al., 1973). Epicontinental marine sedimentation occurred in the Cretaceous (Etayo Serna et al., 1985). During the Miocene, the location of small porphyry bodies with gold mineralization occurred, where the best known are those of the Berlin area (Leal-Mejía, 2011; Mantilla Figueroa et al., 2013). Finally, slope and alluvial deposits formed during the Quaternary.

3.1. Previous studies on Triassic-Jurassic magmatism in the Santander Massif and associated mineralizations

The Late Triassic-Early Jurassic magmatism in the Santander Massif is represented by large batholiths and stocks (Goldsmith et al., 1971; Ward et al., 1973; van der Lelij et al., 2016; Rodríguez et al., 2020a, 2020b). This igneous suite consists mainly of monzogranites and, to a lesser extent, granodiorites, tonalites and diorites (Rodríguez et al., 2017). Basement metamorphic xenoliths are common in some plutons (Rodríguez et al., 2020b). There are also Jurassic and Cretaceous dikes and others that have not yet been dated (Correa Martínez et al., 2020a).

The U–Pb crystallization ages of the Mesozoic igneous units in the Santander Massif are between the Late Triassic (~ 214 Ma) and the Early Jurassic (~ 195 Ma), and contain the following older zircons: from the Proterozoic (1800-1600 Ma, 850-542 Ma), Ordovician-Silurian-Devonian and, to a lesser extent, from the Carboniferous, Permian and Triassic (Goldsmith et al., 1971; Restrepo-Pace et al., 1997; Dörr et al., 1995; Mantilla Figueroa et al., 2013; van der Lelij et al., 2016; Rodríguez et al., 2017; Alarcón-Gómez et al., 2019; Rodríguez et al., 2020a, 2020b).

The magmatism in question ranges from calc-alkaline to high-K calc-alkaline series, is mainly peraluminous and to a lesser extent metalluminous (Mantilla Figueroa et al., 2013; Spikings et al., 2015; van der Lelij et al., 2016; Zuluaga and López, 2019; Rodríguez et al., 2020a). There are two contrasting models that explain this magmatism. First, proponents interpret magmatism as a product of the activity of a continental margin magmatic arc generated in an oblique Pacific subduction zone below the South American margin (Aspden et al., 1987; Restrepo-Pace, 1995; Bayona et al., 2006; Mantilla Figueroa et al., 2013; van der Lelij et al., 2016; Spikings et al., 2015; Rodríguez et al., 2020a). The subduction was framed in an extensional regime related to the fragmentation of Pangea (Restrepo-Pace, 1995; Spikings et al., 2015; van der Lelij et al., 2016). The extension possibly also contributed to the decompression and partial melting of the thinned continental crust (Zuluaga and López, 2019). The peraluminous character has

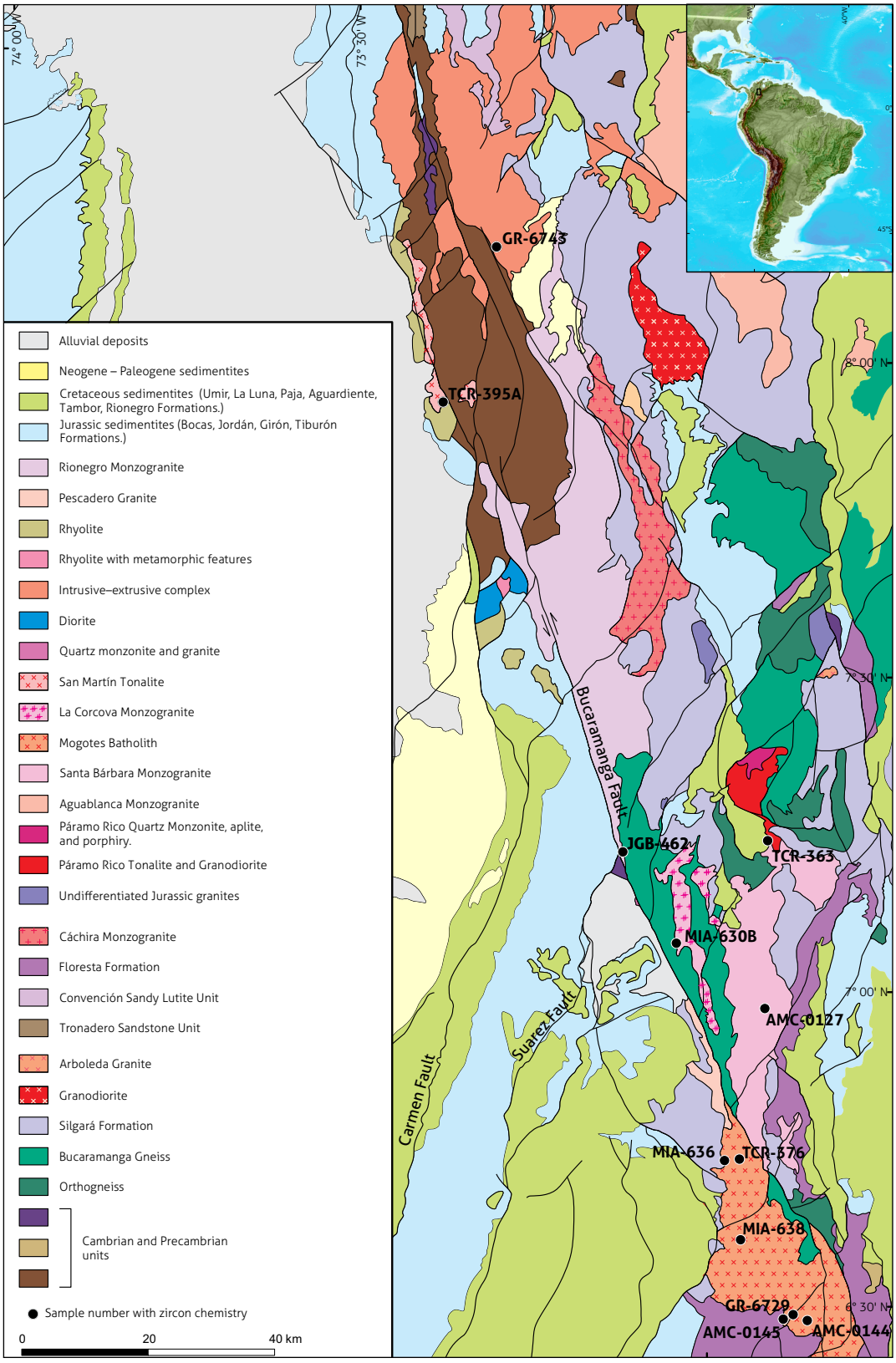

Figure 1. Geological map of the Santander Massif, showing the igneous bodies studied and the location of the analyzed samples
Source: taken from Rodríguez et al. (2020a), modified from Ward et al. (1973).

been interpreted as a result of contamination by the thick continental crust (Spikings et al., 2015; van der Lelij et al., 2016; Zuluaga and López, 2019). From isotopic data collected from Lu–Hf in zircons and Rb–Sr and Sm–Nd in the whole-rock of some of the units studied, van der Lelij et al. (2019) identified that the source corresponded to recycled melts of continental crust of 1 Ga or older at the northwestern end of Gondwana between ~ 472 Ma and ~ 196 Ma, with no contribution of juvenile material. The presence of both peraluminous and metaluminous rocks has been explained as a function of the residence time of the crust in the subduction zone (Mantilla Figueroa et al., 2013). In the second model, other authors interpret that this magmatism was produced by a *rift*-type extension process associated with the fragmentation of Pangea (Kammer, 1993; Mojica et al., 1996) and that said magmatism is not directly associated with subduction (Leal -Mejía et al., 2019). In this sense, the generation of magmas could be related to the partial melting of the metamorphic basement of the Santander Massif, which was thermally induced by the ascent of the mantle as a result of the extensional process (Leal-Mejía et al., 2019).

The available investigations on the potential in metallic mineral deposits of the bodies of the Plutonic Santander Group are few. The main mineralizations investigated thus far are mentioned below: fluorite deposits with galena and quartz are found in lenticular seams in the Pescadero Granite (Willms, 1990; Mantilla Figueroa et al., 2001; Mantilla and Mesa, 2002) and were generated possibly cogenetically with the nesting rock at approximately 200 Ma (Prieto et al., 2019). Fluorite-barite-galena mineralizations are associated with fault zones within the intrusive-extrusive Igneous Complex and correspond to a hydrothermal deposit, but no further details are known about its genesis (Guatame-García, 2009). The presence of Au and Ag in quartz and pyrite veins and minerals rich in rare earth elements are related to hydrothermal alteration processes within the Mogotes Batholith (Gamboa Herrera, 2016). According to Ardila Melo and Ayala Caicedo (2017), the minerals rich in REEs seem to be related to magmatic processes and not to hydrothermal processes.

3.2. Petrographic, geochronological and geochemical summary of the units studied

In this work, the results of samples from the following units are reinterpreted (Figure 1): Mogotes Batholiths (Ward et al., 1973; Correa Martínez et al., 2020a), Santa Bárbara Monzogranite (Ward et al., 1973; Rodríguez et al., 2020c), La Corcova Monzogranite (Ward et al., 1973; Rodríguez et al., 2020d), Páramo Rico Tonalite and Granodiorite (Ward et al., 1973; Rodríguez et al., 2017), Rionegro Monzogranite according to Arango et al. (2020) and an Intrusive-Extrusive Igneous Complex (Daconte and Salinas, 1980), which was considered by Arango et al. (2020) as the northern extension of the Rionegro Monzogranite. Additionally, San Martín Tonalite (Ward et al., 1973; Rodríguez et al., 2020e), San Joaquín Rhyolite (Rodríguez et al., 2020f) and Alto Los Ca-

Table 1. Summary of the petrographic, geochemical and geochronological characteristics of rocks from the Triassic-Jurassic igneous unit of the Santander Massif

SGC ID	Field ID	Latitude N	Length W	Unit	Modal composition/Petrographic classification	Chemical Classification/ Granite Type/Magma Type	U–Pb Age (Ma), MSWD/ Author
900944	MIA-638	6°33'30.56"	72°56'16.53"	Mogotes Batholith	Kfs + Pl + Qtz + Bt + Ap + Op + Zrn/Monzogranite	Granite/"I"/moderately evolved and fractionated	200.4 ± 2.2, MSWD = 6.7/Correa Martínez et al. (2020a)
900962	TCR-376	6°41'06.89"	72°57'13.26"	Mogotes Batholith	Pl + Qtz + Kfs + Bt + Op (Ilm + Mag) + Ap + Zrn/Monzogranite	Granite/"I"/strongly evolved, little fractionated	202.5 ± 1.3, MSWD = 2.6/Correa Martínez et al. (2020a)
900875	AMC-0144	6°25'27.04"	72°50'23.11"	Mogotes Batholith (minor body)	Kfs + Qtz + Pl + Bt + Op + Ms/ Apolytic Sienogranite	Granite/"I"/strongly evolved, fractionated	202.1 ± 1.8, MSWD = 4.6/Correa Martínez et al. (2020a)
900942	MIA-636	6°41'00.04"	72°57'59.63"	Mogotes Batholith (minor body)	Kfs + Pl + Qtz + Bt + Op + Ap + Zrn/Monzogranite	Granite/"I"/moderately evolved, fractionated	205.4 ± 3.0, MSWD = 13/Correa Martínez et al. (2020a)
900890	GR-6729	6°26'37.35"	72°51'22.87"	San Joaquín Rhyolite	Phenocrystals: Pl + Qtz + Bt + Kfs + Op (Ilm + Mag) + Ap + Zrn, felsitic matrix/porphyry Dacite	Rhyolite/"S"/strongly evolved, moderately fractionated	201.0 ± 2.1, MSWD = 3.2/ Rodríguez et al. (2020f)
900876	AMC-0145	6°26'04.10"	72°52'37.26"	Alto Los Cacaos Rhyolites	Spherulitic with felsitic matrix Kfs + Qtz + Pl + Bt + Op (Mag with Ti)/Quartz-trachyte alkaline-porphyry feldspar	Rhyolite/"I"/moderately evolved, fractionated	201.6 ± 2.1, MSWD = 2.3/Correa Martínez et al. (2020b)
900860	AMC-0127	6°56'10.39"	72°54'06.51"	Monzogranite from Santa Barbara (minor body)	Phenocrysts (Pl + Qtz + Bt + Op + Aln + Zrn), vitreous matrix/ Porphyry rhyolite	Rhyolite/"I"/strongly evolved, moderately fractionated	203.0 ± 2.6, MSWD = 9.1/ Rodríguez et al. (2020c)
900936	MIA-630B	7°02'12.09"	73°02'42.73"	La Corcova Monzogranite (minor body, subordinate facies)	Pl + Hbl + Bt + Qtz + Op (Py + Ilm?) + Zrn + Ap + Aln + Tnt/ Quartzodiorite	Diorite/"I"/strongly evolved, little fractionated	207.7 ± 1.2, MSWD = 1.5/ Rodríguez et al. (2020c, 2020d)
900955	TCR-363	7°12'51.56"	72°53'55.72"	Páramo Rico Tonalite and Granodiorite	Pl + Bt + Qtz + Hbl + Kfs + Tnt + Op + Ap + Zrn/Granodiorite	Diorite/"I"/strongly evolved, little fractionated	206.8 ± 1.0, MSWD 1.1/Rodríguez et al. (2017)
900938	MIA-632	7°12'38.33"	73°07'43.86"	Rionegro Monzogranite	Pl + Qtz + Kfs + Bt + Op (Ilm?) + Tnt + Ap + Zrn + Aln/Granodiorite	Granite/"I"/strongly evolved, moderately fractionated	Sample with trace elements JGB-462: 197.2 ± 1.5, MSWD = 3.0/ Arango et al. (2020)
900973	GR-6743	8°11'22.43"	73°19'00.39"	Intrusive-Extrusive Igneous Complex (Rionegro Monzogranite according to Arango et al. (2020))	Pl + Qtz + Kfs + Bt + Op + Ap + Zrn + Tnt/Granodiorite-monzogranite	Granite/"I"/moderately evolved, little fractionated	195.9 ± 1.6, MSWD = 4.0/Arango et al. (2020)
901032	TCR-395A	7°55'41.61"	73°23'44.42"	San Martín Tonalite	Pl + Qtz + Bt + Hbl + Kfs + Op (Mag + Py) + Zrn + Ap/Tonalite	Quartzodiorite-granodiorite/"I"/ not evolved, not or little fractionated	198.9 ± 1.8, MSWD = 1.1/ Rodríguez et al. (2020e)

Mineral abbreviations: Whitney and Evans (2010).

caos Rhyolites (Correa Martínez et al., 2020b) are also present. The location of the studied samples is shown in Figure 1.

Detailed petrographic descriptions and geochemical and geochronological characterizations of the units can be found in the works cited in the previous paragraph. Table 1 summarizes the petrographic composition, the petrographic and chemical classifications and the ages of the samples studied.

The lithotypes analyzed were mainly monzogranites and, to a lesser extent, porphyry rhyolites, quartzodiorites or diorites and granodiorites. All the samples are from the subalkaline series, with a high-K calc-alkaline trend, except for the San Martín Tonalite (TCR-395) sample, which follows the calc-alkaline trend (Rodríguez et al., 2017). Most of the samples are peraluminous and slightly peraluminous (ACNK <1.1), and only samples MIA-630B (La Corcova Monzogranite), TCR-363 (Páramo Rico Tonalite and Granodiorite) and GR-6743 (Intrusive-Extrusive Igneous Complex) are metaluminous (Rodríguez et al., 2017, 2020b).

4. Methods

In this work, the zircon trace-element composition of several samples published in the following studies was reinterpreted: Rodríguez et al. (2017, 2020c, 2020d, 2020e, 2020f), Correa Martínez et al. (2020a, 2020b) and Arango et al. (2020). The analysis was conducted on zircons with Triassic-Jurassic ages; therefore, xenocrystals were excluded. For the fertility interpretations, zircons with La> 1 ppm and Ti> 50 ppm were discarded since those values may reflect inclusions of apatite and Ti- (Fe-) oxides, respectively (Lu et al., 2016).

The Eu anomaly was obtained by the following formula: $Eu/Eu^{\star} = Eu_{N}/(Sm_{N} \times Gd_{N})^{0.5}$. The Ce anomaly was calculated by the method presented in Loader et al. (2017) using the following equation: $Ce/Ce^{\star} = Ce_{N}/[(Nd_{N})^{2}/Sm_{N}]$. The subscript N denotes the values normalized to those of the chondrite presented in Sun and McDonough (1989).

5. Results

5.1. Zircon geochemistry

The complete results of the reinterpreted samples can be found in Rodríguez et al. (2017, 2020c, 2020d, 2020e, 2020f), Correa Martínez et al. (2020a, 2020b) and Arango et al. (2020). Table 2 summarizes the maximum, minimum and median values of the chemical elements and ratios of zircons.

Table 2. Summary of the statistics of the chemical composition of igneous zircons associated with the crystallization events of the Late Triassic-Early Jurassic

Sample	MIA-638			TCR-376			MIA-636			AMC-0144			GR-6729			AMC-0145		
Age range (Ma)	214.8-195.1 (n = 12)			217.3-196.4 (n = 21)														
Main population age	206.2-198.7 (n = 9)			207.1-196.4 (n = 19)			219.4-199.1 (n = 16)			208.2-196.7 (n = 14)			209.4-191.9 (n = 13)			213.4-195.2 (n = 16)		
Trace element	Min	Median	Max.	Min	Median	Max.	Min	Median	Max.	Min	Median	Max.	Min	Median	Max.	Min	Median	Max.
You	6	8.25	15.9	6.61	8.26	13.17	6.71	10.45	17.8	5.37	7.48	10	7.1	13.10	22.3	7.35	10.50	13.5
P	320	1040.00	3510	72	248.00	970	160	505.00	1130	11	210.00	340	-	-	-	53	363.00	580
And	632	2545.00	9800	370	1433.00	6140	721	1685.00	4480	472	1105.00	2350	550	1460.00	4100	876	1330.00	2280
Nb	3.62	10.05	86	1.89	4.97	28.1	1.21	6.45	70.8	1.34	4.80	8.3	1.3	2.83	8	1.26	3.59	15
The	0	0.16	0.51	0	0.07	0.33	0.0015	0.08	0.87	bdl	0.01	0.46	0	0.03	0.49	bdl	0.03	0.64
Ce	17	121.50	689	16.1	51.30	424	16	65.80	155	18.1	43.75	93	16.6	33.30	122	22.1	44.85	58.2
Pr	0.028	0.34	1.15	0.0037	0.14	1.6	0.074	0.14	0.56	0.0159	0.07	0.7	0.039	0.26	1.22	0.055	0.24	0.61
Nd	0.59	5.48	22.7	0.26	3.03	25.2	1.44	2.95	9.8	0.38	1.48	9.7	0.69	2.80	16.3	1.48	4.05	8.8
Sm	1.45	9.85	46.7	0.7	5.10	41.6	2.94	5.86	15.9	1.21	3.02	16.2	1.58	5.60	27.7	3.26	6.98	13.4
Eu	0.466	3.49	11.8	0.314	2.25	10.59	0.98	1.89	4.55	0.451	1.16	5.2	0.61	1.76	8.9	1.29	2.24	5.04
Gd	9.5	49.85	255	4.8	24.70	184.6	14.9	34.75	84	8.24	18.40	66.2	10	28.00	124	21.3	35.20	59.5
Tb	3.45	17.25	85	2.05	8.71	54.2	5.13	12.25	29.8	3.06	6.38	19.5	3.8	10.60	38	6.86	11.50	19.1
Dy	45.1	205.00	960	27.3	115.30	606	62.2	153.00	405	38	83.55	218	46.4	128.00	420	81	137.50	217
Ho	19.7	82.85	352	11.8	49.70	217	23.9	59.20	158	14.8	34.50	76	19.1	50.00	146	28.6	45.85	78.3
Er	98	377.00	1460	60.5	219.60	911	115	266.50	738	76.1	175.00	371	88	230.00	590	140	211.50	366
Yb	274	785.00	2320	151	484.90	1540	244	518.00	1350	184	417.00	781	181	460.00	1020	275	385.00	690
Mon	64	161.50	437	35.9	101.20	293	50.3	106.35	257	42.1	90.75	164	37.1	96.00	201	57.1	79.25	139
Hf	7000	9800.00	17 500	7940	10 770.00	11 340	7330	10 225.00	14 100	8470	10 550.00	11 700	7100	9300.00	14 300	7630	9040.00	10 700
Pb	7.775	15.45	66.25	4.025	11.98	41.75	1.5125	6.66	47.5	4.975	11.10	23	1.525	4.33	11.25	2.1275	6.05	13.35
Th	208	618.00	7070	71.5	389.00	3570	47.1	208.50	1360	105.8	312.50	920	50.6	198.00	590	73.4	184.00	353
U	234	466.00	1990	118	355.60	1242	45.6	209.00	1550	148	357.00	724	44.2	133.00	335	68.8	182.50	382
Eu/Eu*	0.25	0.37	0.61	0.37	0.48	0.62	0.20	0.44	0.62	0.36	0.47	0.52	0.39	0.47	0.54	0.40	0.45	0.56
Ce/Ce*	26.10	151.40	795.07	13.20	150.38	394.13	20.7	98.38	455.3	30.1	170.37	471.3	11.33	50.88	163.86	17.9	46.08	238.9
10 000*(Eu/Eu*)/Y	0.34	1.63	4.54	0.60	4.09	14.15	0.45	2.84	7.13	1.85	4.38	9.25	1.13	2.69	8.53	1.86	3.50	5.09
(Ce/Nd)/Y	0.003	0.010	0.063	0.002	0.021	0.167	0.003	0.010	0.026	0.003	0.027	0.101	0.001	0.01	0.056	0.003	0.008	0.032
Dy/Yb	0.19	0.30	0.41	0.18	0.23	0.39	0.25	0.30	0.37	0.18	0.22	0.35	0.25	0.33	0.41	0.25	0.31	0.39

Sample	AMC-0127			MIA-630B			TCR-363			JGB-462			GR-6743			TCR-395A		
Age (Ma)	212.7-194.3 (n = 18)			212.6-196.3 (n = 31)			214.0-200.9 (n = 28)			205.6-187.8 (n = 26)			204.7-186.4 (n = 21)			205.1-194.5 (n = 11)		
Trace element	Min	Median	Max.	Min	Median	Max.	Min	Median	Max.	Min	Median	Max.	Min	Median	Max.	Min	Median	Max.
You	7.3	9.00	12.9	5.86	7.68	32.8	6.55	8.52	14.1	7	9.0	14	6.53	9.87	14.7	7.13	8.71	13.67
P	135	336.50	2260	31	317.00	888	-	230.00	560	257	496.0	1033	140	526.00	1820	300	644.00	884
And	628	1485.50	6470	606	2280.00	7090	232	695.50	1850	740	1890.5	4560	621	2060.00	7360	938	2220.00	3208
Nb	0.99	4.07	16.3	2.11	11.80	40.8	0.71	1.72	5.6	2	7.0	15	2.01	6.16	39.4	2.14	3.75	5.87
The	0	0.03	0.282	bdl	0.06	0.81	0	0.00	0.65	0	0.0	0	0	0.06	0.53	0.0019	0.07	0.311
Ce	21.94	41.65	94	38	199.00	629	7.7	25.50	60.1	17	65.5	188	21.83	58.30	262	11.29	25.10	37.6
Pr	0.035	0.12	0.69	0.042	0.32	2.4	0.0051	0.05	0.276	0	0.0	2	0.022	0.18	0.73	0.052	0.15	0.39
Nd	0.76	2.15	10.2	0.74	4.51	32.6	0.29	0.99	5.71	1	2.5	23	0.75	3.47	12	0.52	2.52	6.83
Sm	2.43	5.46	15.6	1.29	8.06	43.3	0.29	2.26	11.1	2	6.0	30	1.28	6.10	26.9	1.77	5.31	13.14
Eu	0.77	1.77	5.6	0.66	2.90	14.6	0.203	0.74	3.77	1	2.0	9	0.61	2.26	7.33	0.375	1.47	5.45
Gd	12.3	29.20	73.5	8.8	43.90	181	2.64	11.40	49.5	11	33.5	114	8.42	38.00	151.1	13.7	39.50	69.5
Tb	4.23	10.09	36.1	3.75	14.40	55.6	1.14	4.07	14.9	4	12.5	38	3.28	13.68	54	5.71	14.32	23.73
Dy	53.7	125.20	541	46	183.00	632	14.9	49.95	163	59	159.0	431	43.1	168.90	648	74.8	185.00	280.3
Ho	20.7	49.00	221	18.8	72.70	231	6.96	21.90	60.7	25	62.5	162	18.75	66.00	246.6	31	74.10	108.9
Er	96.6	232.25	1040	92	332.00	1030	38.8	112.10	294	120	301.5	718	100	312.00	1073	151.4	346.00	482.8
Yb	196.9	475.15	2170	218	765.00	2280	114	290.50	676	271	632.5	1271	260	675.00	1910	322	701.00	937
Mon	42.6	99.40	399	52.1	162.00	468	29	69.10	150	59	137.0	255	62.4	148.70	361	68.2	144.10	193.9
Hf	8692	10 135.00	14 630	7090	8850.00	13 800	8500	11 100.00	13 300	6228	7974.5	10 036	8110	9790.00	11 800	7333	9580.00	11 450
Pb	5.9	14.69	75.25	13.975	51.25	102.5	2	8.95	27.75	1.75	5.3	33.5	2.095	8.04	20.05	1.0275	2.57	3.48
Th	163.2	324.50	960	511	2790.00	10330	62	188.00	705	66	257.5	858	71.1	284.40	1000	19.9	70.10	104
U	183	437.30	2260	404	1510.00	3180	56.5	272.00	844	53	157.5	1021	62.8	261.20	630	31.8	77.00	100.1
Eu/Eu*	0.14	0.47	0.57	0.38	0.49	0.62	0.30	0.48	0.71	0.17	0.43	0.65	0.28	0.47	0.61	0.17	0.29	0.55
Ce/Ce*	12.6	115.89	610.9	40.5	176.91	471.0	22.9	95.00	498.4	12.5	118.78	321.4	10.7	80.35	713.3	13.9	59.01	172.1
10 000*(Eu/Eu*)/Y	0.33	3.24	8.32	0.7	1.95	8.4	2.09	6.79	30.57	0.64	2.14	8.81	0.45	1.96	9.15	0.72	1.31	2.48
(Ce/Nd)/Y	0.002	0.016	0.063	0.002	0.017	0.078	0.003	0.03	0.154	0.001	0.012	0.043	0.002	0.008	0.043	0.001	0.005	0.023
Dy/Yb	0.21	0.27	0.36	0.13	0.26	0.34	0.13	0.19	0.37	0.21	0.26	0.39	0.17	0.25	0.35	0.22	0.26	0.31

bdl: below detection limit.

The REE patterns obtained for zircons with ages between the Late Triassic and the Early Jurassic are shown in Figure 2. Most of the patterns exhibit the shape characteristic of magmatic zircon patterns with negative Eu anomalies and positive Ce anomalies. It is observed that some REE patterns show enrichment in light REE (LREE; represented with dotted and colored lines), which may be due to the inclusions of REE-bearing minerals, such as apatite or monazite, which is a common type of contamination when analyzing zircons by laser ablation inductively coupled plasma mass spectrometry (LA-ICP-MS) (Lu et al., 2016). With the exception of the zircons from sample TCR-395A, the zircons from the other samples, in general, exhibit mild negative Eu and pronounced positive Ce anomalies.

The fertility indicators, according to Lu et al. (2016), for Cu porphyry systems (±Mo±Au) are shown in Figure 3. The meaning of the variables of each of the diagrams are explained in the section "Background on metallogenetic fertility potential of magma". The zircons of almost all the samples display Eu/Eu* ratios above 0.3, and many show (Ce/Nd)/Y values greater than 0.01 (Figures 3a, 3b and medians presented in Table 2), which plot in fertile magma field for Cu (±Mo±Au). This indicates that they were derived from magmas with high water content or high oxidation states or both. There are exceptions, such as the San Martín Tonalite, in which a large part of its zircons exhibits Eu/Eu* values below 0.3 and (Ce/Nd)/Y values less than 0.01; thus, following the criteria presented by Lu et al. (2016), these would represent nonhydrated and reduced magmas. Regarding the relationship 10 000* (Eu/Eu*)/Y (Figures 3c, 3d and medians in Table 2), the zircons from most samples have values greater than 1, which indicates the derivation of hydrated and fertile magmas with fractionation of amphibole and suppression of plagioclase; however, by again applying this criterion, the zircons of the San Martín Tonalite plot at the limit, slightly above 1. For the relationship of Eu/Eu* and Dy/Yb (Figures 3e, 3f and medians presented in Table 2), it can be seen that most zircons have Dy/Yb values less than or equal to 0.3 and Eu/Eu* greater than 0.3, which indicates early and late fractionation of amphibole and plagioclase, respectively. In the diverse diagrams (Figure 3), these zircons plot within the fields of fertile suites. Some zircons of the samples from the

Mogotes Batholith, the Rionegro Monzogranite, the La Corcova Monzogranite and most of the zircons from the San Joaquín rhyolite and the Alto Los Cacaos rhyolites exhibit values greater than 0.3, which suggests that there was no early amphibole fractionation, and from this criterion, they would derive from infertile magmas.

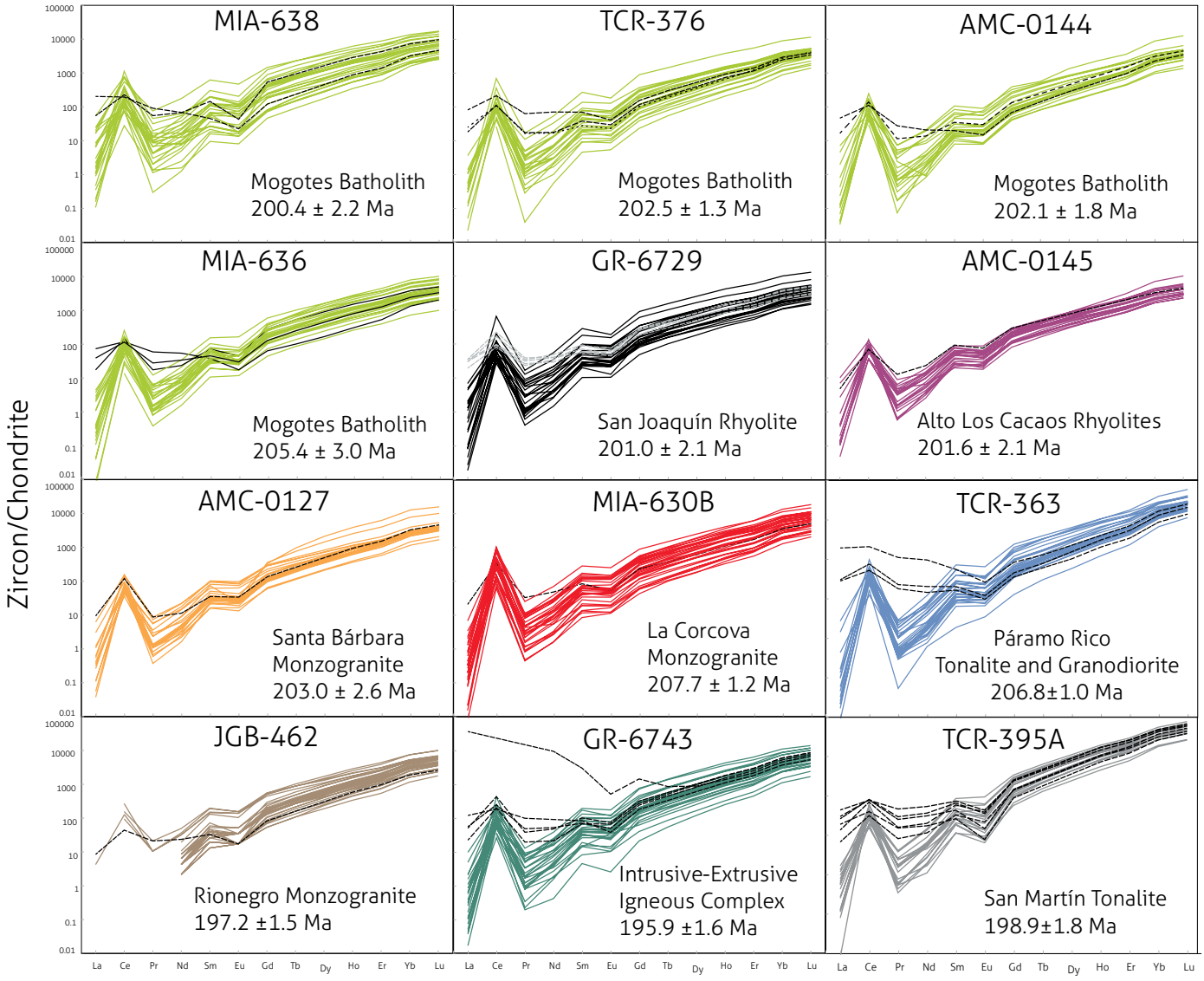

Figure 2. REE patterns of zircons with ages between the late Triassic and the early Jurassic
Normalization values are those of the chondrites presented in Sun and McDonough (1989). Dashed lines correspond to the standards enriched in LREEs. Source of the ages presented in Table 1.

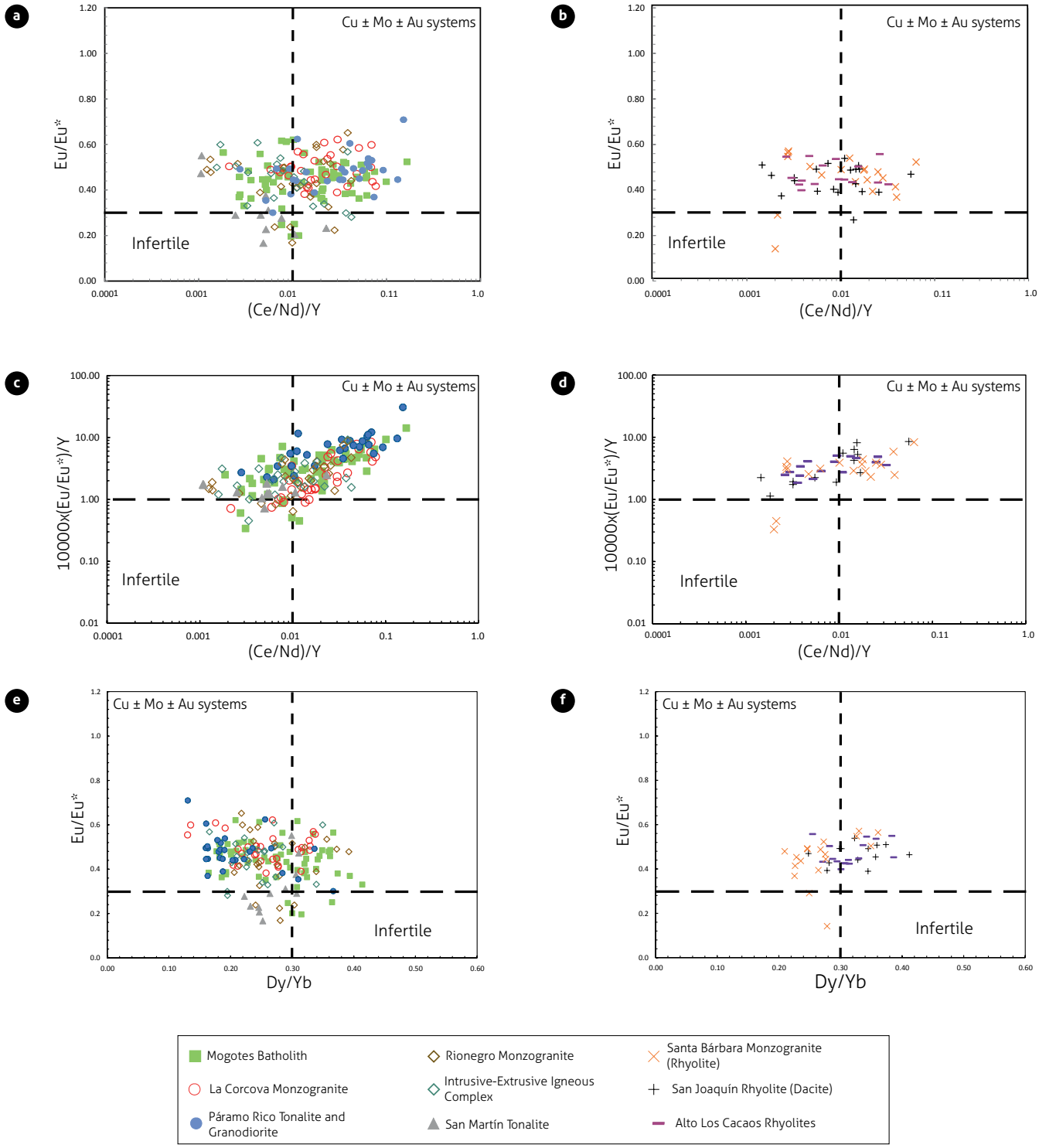

Figure 3. Chemical composition of the zircons of Triassic-Jurassic units of the Santander Massif presented in diagrams from Lu et al. (2016), which are used to discriminate potential fertility in Cu ±Mo±Au deposits
a) Plot of zircon Eu/Eu* vs. (Ce/Nd)/Y from equigranular rocks; b) plot of zircon Eu/Eu* vs. (Ce/Nd)/Y from porphyry rocks; c) plot of zircon 10 000* (Eu/Eu*)/Y vs. (Ce/Nd)/Y from equigranular rocks; d) plot of zircon 10 000* (Eu/Eu*)/Y vs. (Ce/Nd)/Y from porphyry rocks; e) plot of zircon Eu/Eu* vs. Dy/Yb from equigranular rocks; f) plot of zircon Eu/Eu* vs. Dy/Yb from porphyry rocks.

Lu et al. (2016) found that the Ce/Nd ratios in zircon overlap between fertile and infertile suites within the range ~3-~13, suggesting that this relationship may not be a good proxy of the oxidation state of the melt. To obtain another approximation of the oxidation state of the studied samples, the Ce anomaly was calculated as explained in the methods section (Table 2, Figure 4). Qualitatively, the source magmas of the San Joaquín and Alto Los Cacaos rhyolites and the San Martín Tonalite were the least oxidized. The intermediate oxidation magmas generated the rocks of the Intrusive-Extrusive Igneous Complex, the Páramo Rico Tonalite and Granodiorite, a sample of the Mogotes Batholith (MIA-636), and the Santa Bárbara and Rionegro monzogranites. Lastly, the most oxidized were the source magmas of the three samples of the Mogotes Batholith (MIA-638, TCR-376, and AMC-0144) and the diorite of the La Corcova Monzogranite (MIA-630B).

The relative degrees of fractionation and hydration of the magmas, indicated by the Eu anomaly (Table 2, Figure 4) can be interpreted as follows: San Martín Tonalite represents the most fractionated and least hydrated magma followed, in order of decreasing degree of fractionation and increasing of hydration, by sample MIA-638 from the Mogotes Batholith and the other samples, which are grouped with lower degrees of fractionation and higher degrees of hydration. The relatively less fractionated and more hydrated magma was that from La Corcova.

6. Discussion

6.1. Metallogenetic fertility potential of the Triassic-Jurassic magmatism of the Santander Massif

The REE patterns with pronounced positive Ce and slight negative Eu anomalies in almost all samples (Figure 2), except in TCR-395, could suggest that they crystallized in oxidized magmatic systems, where there was suppression of the previous plagioclase crystallization, which are systems with greater fertility potential for porphyry-type copper mineralizations (Ballard et

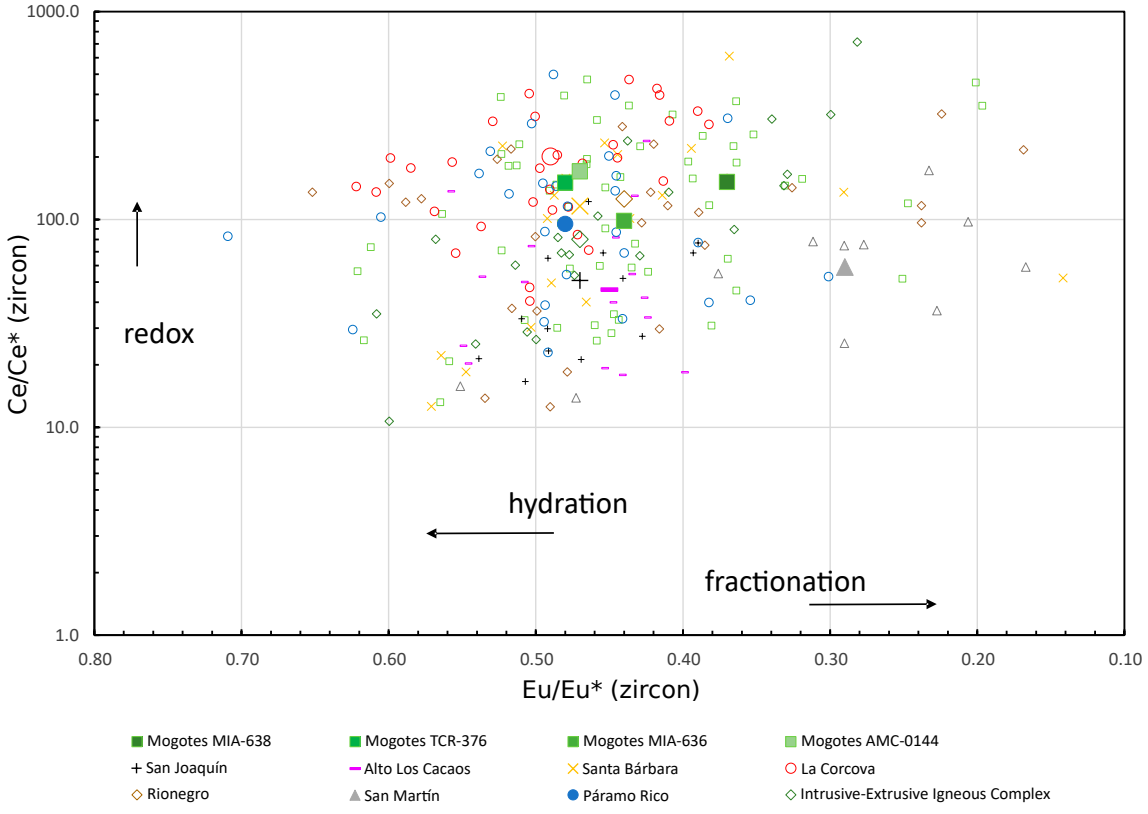

Figure 4. Zircon Ce/Ce* vs. Eu/Eu* plot
Small symbols and light colors correspond to all the zircons of the respective samples. Larger symbols and stronger colors represent the medians of the Eu and Ce anomalies for each of the samples tested. Source: adapted from Gardiner et al. (2017).

al., 2002; Richards et al., 2012; Chelle-Michou et al., 2014; Dilles et al., 2015; Lu et al., 2016). However, this characteristic of the Eu anomaly in some samples may also be due to the prior or co-crystallization of titanite with zircon (Loader et al., 2017). The samples in which this process could occur are those From La Corcova Monzogranite (MIA-630B), Páramo Rico Tonalite and Granodiorite, the Rionegro Monzogranite (JGB-462) and the Intrusive-Extrusive Igneous Complex (GR-6743) because they contain modal titanite (see Table 1). However, if the negative Eu anomaly was made less pronounced by the crystallization of titanite, the presence of this mineral is also an indicator of potential Cu porphyry fertility (Loader et al., 2017).

Of the samples from the Mogotes Batholith, TCR-376 and AMC-0144 have the highest Eu/Eu* and 10 000* (Eu/Eu*)/Y ratios (Table 2, Figures 3a, 3c), indicating high contents of magmatic water; therefore, they would be more hydrated and have less magmatic fractionation than the MIA-636 and MIA-638 samples (Figure 4). According to the 10 000* (Eu/Eu*)/Y ratio, there was greater early amphibole fractionation in sample AMC-0144, later fractionation in samples TCR-376 and MIA-636, and minimal early amphibole fractionation in MIA-638. These results are similar to those obtained by the Dy/Yb ratio (Table 2, Figure 3e), which, similar to the previous results, reflects the early fractionation of amphibole. Of the four samples, the most fractionated and least hydrated is MIA-638 (Figure 4). Regarding the oxidation state based on the ratio (Ce/Nd)/Y, samples AMC-0144 and TCR-736 show values greater than 0.01, that is, oxidized, while MIA-638 and MIA-636 have values equal to 0.01. Additionally, according to the Ce/Ce* ratio, MIA-636 is less oxidized, and the other three have similar oxidation states (Table 2; Figures 3a, 3c, 4). The samples TCR-376 and AMC-0144 have higher fertility potential for the porphyry-type Cu (±Mo±Au) deposits within the Mogotes Batholith because they are more hydrated and oxidized and have less magmatic fractionation than the other two.

The samples from the San Joaquín (GR-6729) Rhyolite, Alto Los Cacaos Rhyolites (AMC-0145), and Santa Bárbara Monzogranite (AMC-0127) show similar degrees of hydration and fractionation according to the Eu/Eu* and 10 000* (Eu/Eu*)/Y values (Table 2; Figures 3 b, 3d, 4). When considering the Dy/Yb ratio, there was early amphibole fractionation in the AMC-0127 sample (Figure 3f). This sample, according to the relationships (Ce/Nd)/Y and Ce/Ce* (Table 2; Figures 3b, 3d, 4), also exhibits a higher oxidation state compared to the other two. In this subset of samples, AMC-0127 has the highest fertility potential for Cu (±Mo±Au) porphyry-type deposits, mainly due to its higher oxidation state.

Samples from La Corcova Monzogranite (MIA-630B), Páramo Rico Tonalite and Granodiorite (TCR-363), Rionegro Monzogranite (JGB-462), and Intrusive-Extrusive Igneous Complex (GR-6743) show relatively similar hydration states, according to the Eu/Eu* ratio, being higher in MIA-630B, followed by TCR-363, GR-6743, and JGB-462. Early amphibole fractionation was significant in sample TCR-363 for its comparatively higher values of the 10 000*(Eu/Eu*)/Y and Dy/Yb ratios. Starting from the Ce/Ce* ratio in decreasing order of oxidation state were: MIA-630B, JGB-462, TCR-363, and GR-6743; while according to the (Ce/Nd)/Y ratio, the decreasing order varies as follows: TCR-363, MIA-630B, JGB-462, and GR-6743. Samples MIA-630B, TCR-363, and GR-6743 are less fractionated than JGB-462. Of this group, the two with the highest fertility potential for porphyry-type Cu (±Mo ±Au) deposits are MIA-630B and TCR-363.

In the case of the San Martín Tonalite, the ratio Eu/Eu* would indicate that it is less hydrated than the other samples analyzed (Table 2; Figures 3a, 4). The values of the 10 000* (Eu/Eu*)/Y (> 1) and Dy/Yb (<0.3) ratios (Figures 3c, 3d) are consistent with amphibole fractionation, but this process did not occur simultaneous with suppression of the plagioclase crystallization. According to the zircon Eu anomaly (<0.3), this sample presents a higher degree of magmatic fractionation (Figure 4), possibly because crystallization occurred, as well as an early accumulation of plagioclase (as indicated by a positive Eu anomaly in the REE pattern for the total rock (Rodríguez et al., 2020e)). These processes could have impoverished in Eu the melt from which the zircon subsequently crystallized. Of all the samples analyzed, this exhibits the lowest degree of hydration and a low oxidation state, and, although comparable with that of the samples from San Joaquín and Alto Los Cacaos, the highest degree of magmatic fractionation; therefore, it does not offer a high fertility potential for porphyry-type Cu (±Mo±Au) deposits.

By integrating the information of the Ce and Eu anomalies within the normalized REE patterns and in the diagram proposed by Gardiner et al. (2017) and the fertility indicators proposed by Lu et al. (2016) (Table 2; Figures 2, 3 and 4), it is possible to interpret that, with the exception of the San Martín Tonalite, the studied samples from the Santander Massif show a variable metallogenic fertility potential for metals from porphyry-type Cu (±Mo±Au) deposits. This potential is greater

in the samples that represent more hydrated magmas, where suppression of the previous plagioclase crystallization and early amphibole fractionation possibly occurred. Furthermore, these samples represent more oxidized magmas and with little fractionation magmatic.

According to the results obtained (Table 2; Figures 3, 4), a relative metallogenetic fertility potential is proposed for Cu(±Mo±Au) mineralizations. The dioritic facies of the La Corcova Monzogranite and the Páramo Rico Tonalite and Granodiorite exhibit the highest fertility potential. They follow, in decreasing order of fertility potential, those of the Mogotes Batholith (inside this unit, there are variable hydration and oxidation and, consequently, fertility characteristics), the Rionegro Monzogranite, the Intrusive-Extrusive Igneous Complex and a minor body within the Santa Bárbara Monzogranite. Due to the redox state, the samples from the San Joaquín Rhyolite and Alto Los Cacaos Rhyolites would not be very fertile, while the tonalite from San Martín would be less fertile or infertile.

Units that are not very fertile or infertile in terms of Cu (±Mo±Au) mineralizations could be fertile for other types of mineralizations, such as for W or Sn. Analysis of this potential requires information from additional trace elements within the zircon, which are not available for the samples studied.

The potential of metallogenetic fertility for porphyry-type Cu (±Mo±Au) deposits from the investigated units opens the possibility of delimiting areas for future exploration, which could verify the occurrence of these mineral deposits. However, it is important to note that the fertility potential does not determine whether these mineralizations exist or have existed. It is probable that they are not yet exposed, that they have been eroded or that, due to other tectono-magmatic factors, such as those mentioned in the section "Background on metallogenetic fertility potential of magma", the mineralizations would not have been developed.

7. Conclusions

According to the chemical composition of the zircons from various Triassic-Jurassic magmatic units of the Santander Massif, it is possible to conclude that a large part of this magmatism exhibits metallogenic fertility potential for porphyry-type Cu (±Mo±Au) deposits.

The combination of variables such as degrees of hydration and fractionation and redox state perhaps gave a different metallogenic fertility potential for each magmatic source. The rocks with fertility potential derived from magmas that were hydrated, oxidized, and underwent relatively little magmatic fractionation. The degree of hydration perhaps allowed for early amphibole fractionation and late plagioclase fractionation.

According to the results, and in a relative way, the bodies with the highest fertility potential for Cu (±Mo±Au) mineralizations correspond to the dioritic facies of La Corcova and the tonalite and granodiorite unit of Páramo Rico. The Mogotes batholith has a variable potential between intermediate and low. The units that exhibit intermediate potential are the intrusive-extrusive igneous complex, and the monzogranite of Rionegro and Santa Bárbara. The units of San Joaquín rhyolite and the Alto Los Cacaos rhyolites exhibit low potential. The San Martín tonalite is the unit with the lowest fertility potential for Cu (±Mo±Au) mineralization.

The analysis of the fertility potential carried out in this study allows us to define bodies and regions as exploration targets. Metallogenic fertility potential in Cu(±Mo±Au) deposits could be contrasted and verified by detailed exploration methods.

Acknowledgments

This work was supported by the Servicio Geológico Colombiano, which financed the "Jurassic Magmatism in Colombia" project. We thank the anonymous reviewers for their critical and constructive reviews.

Supplementary Data

Supplementary data for this article can be found online at https://doi.org/10.32685/0120-1425/bol.geol.50.1.2023.664

References

Alarcón-Gómez, C. M., Rodríguez-Lizcano, J. G., Clavijo-Torres, J., & Mantilla, L. C. (2019). Geocronología de las rocas volcánicas de la Formación Jordán y su relación con el magmatismo del Jurásico temprano en el Macizo de Santander. In *XVII Congreso Colombiano de Geología. IV Simposio de Exploradores. Geología en tierra de Paz* (pp. 1039-1042). Sociedad Colombiana de Geología.

Arango, M. I., Rodríguez, G., Zapata, G., & Correa Martínez, A. M. (2020). Monzogranito de Rionegro. In *Catálogos de las unidades litoestratigráficas de Colombia: Macizo de Santander*. Vol. 1. Servicio Geológico Colombiano. https://doi.org/10.32685/9789585279445.5

Ardila Melo, D. H., & Ayala Caicedo, A. C. (2017). *Estudio mineralógico-petrográfico de las alteraciones hidrotermales presentes en las rocas ígneas aflorantes a lo largo de la transecta Mogotes - San Joaquín (Macizo de Santander, Colombia)* (Bachelor Thesis). Facultad de Ingeniería Físico-Químicas, Universidad Industrial de Santander.

Aspden, J. A., McCourt, W. J., & Brook, M. (1987). Geometrical control of subduction-related magmatism: The Mesozoic and Cenozoic plutonic history of western Colombia. *Journal of the Geological Society, 144*(6), 893-905. https://doi.org/10.1144/gsjgs.144.6.0893

Ballard, J. R., Palin, M. J., & Campbell, I. H. (2002). Relative oxidation states of magmas inferred from Ce(IV)/Ce(III) in zircon: Application to porphyry copper deposits of northern Chile. *Contributions to Mineralogy and Petrology, 144*(3), 347-364. https://doi.org/10.1007/s00410-002-0402-5

Bayona, G., Rapalini, A., & Costanzo-Álvarez, V. (2006). Paleomagnetism in Mesozoic rocks of the northern Andes and its implications in Mesozoic tectonics of northwestern South America. *Earth, Planets and Space, 58*(10), 1255-1272. https://doi.org/10.1186/BF03352621

Belousova, E. A., Griffin, W. L., & O'Reilly, S. Y. (2006). Zircon crystal morphology, trace element signatures and Hf isotope composition as a tool for oetrogenetic modelling: Examples from Eastern Australian granitoids. *Journal of Petrology, 47*(2), 329-353. https://doi.org/10.1093/petrology/egi077

Blevin, P. L., & Chappell, B. W. (1992). The role of magma sources, oxidation states and fractionation in determining the granite metallogeny of eastern Australia. *Transactions of the Royal Society of Edinburgh: Earth Sciences*, *83*(1-2), 305-316. https://doi.org/10.1017/S0263593300007987

Blevin, P. L., & Chappell, B. W. (1995). Chemistry, origin, and evolution of mineralized granites in the Lachlan fold belt, Australia; the metallogeny of I- and S-type granites. *Economic Geology, 90*(6), 1604-1619. https://doi.org/10.2113/GSECONGEO.90.6.1604

Blevin, P. L., Chappell, B. W., & Allen, C. M. (1996). Intrusive metallogenic provinces in eastern Australia based on granite source and composition. *Earth Sciences, 87*(1-2), 281-290. https://doi.org/10.1017/s0263593300006684

Burnham, A. D., & Berry, A. J. (2012). An experimental study of trace element partitioning between zircon and melt as a function of oxygen fugacity. *Geochimica et Cosmochimica Acta*, *95*, 196-212.

Cediel, F. (1969). Geología del Macizo de Floresta. In *Resúmenes I Congreso Colombiano de Geología* (pp. 17-29).

Chappell, B. W., & White, A. J. R. (1974). Two contrasting granite types. *Pacific Geology*, 8, 173-174.

Chelle-Michou, C., Chiaradia, M., Ovtcharova, M., Ulianov, A., & Wotzlaw, J. F. (2014). Zircon petrochronology reveals the temporal link between porphyry systems and the magmatic evolution of their hidden plutonic roots (the Eocene Coroccohuayco deposit, Peru). *Lithos*, *198-199*(1), 129-140. https://doi.org/10.1016/j.lithos.2014.03.017

Cheng, Y., Spandler, C., Chang, Z., & Clarke, G. (2018). Volcanic-plutonic connections and metal fertility of highly evolved magma systems: A case study from the Herberton Sn-W-Mo mineral field, Queensland, Australia. *Earth and Planetary Science Letters, 486*, 84-93. https://doi.org/10.1016/j.epsl.2018.01.012

Chiaradia, M., Ulianov, A., Kouzmanov, K., & Beate, B. (2012). Why large porphyry Cu deposits like high Sr/Y magmas? *Scientific Reports*, *2*(1), 1-7. https://doi.org/10.1038/srep00685

Cooke, D. R., Kitto, P. A., Harris, A. C., Chang, Z., Wilkinson, J. J., Wilkinson, C. C., Hollings, P., & Webster, J. D. (2009). Magma fertility and mineralisation. In *Proceedings of the 10th Biennial Meeting of the the SGA 2009*, (1), 8-10. Smart Science for Exploration and Mining: 10th Biennial Meeting of the SGA 2009, August 17-20, 2009, Townsville, Australia.

Cooke, D. R., Agnew, P. D., Hollings, P., Baker, M. J., Chang, Z., Wilkinson, J. J., White, N. C., Zhang, L., Thompson, J., Gemmell, J. B., Fox, N., Chen, H., & Wilkinson, C. C. (2017). Porphyry indicator minerals (PIMS) and porphyry vectoring and fertility tools (PVFTS). In *Proceedings of Exploration 17: Sixth Decennial International Conference on Mineral Exploration 2017,* 457-470. Exploration '17: Sixth Decennial International Conference on Mineral Exploration, October 22-25, 2017, Toronto, Canadá.

Cordani, U. G., Cardona, A., Jiménez, D., Liu, D., & Nutman, A. P. (2005). Geochronology of Proterozoic basement inliers in the Colombian Andes: Tectonic history of remnants of a fragmented Grenville belt. In A. P. M. Vaughan, P. T. Leat, & R. J. Pankhurst (eds.), *Terrane processes at the margins of Gondwana* (pp. 329-346). Geological Society of London. https://doi.org/10.1144/GSL.SP.2005.246.01.13

Correa Martínez, A. M., Rodríguez, G., Arango, M. I., Zapata, G., & Bermúdez, J. G. (2020a). Batolito de Mogotes. In *Catálogos de las unidades litoestratigráficas de Colombia: Ma-*

cizo de Santander. Vol. 1. Servicio Geológico Colombiano. https://doi.org/10.32685/9789585279445.1

Correa Martínez, A. M., Rodríguez, G., Bermúdez, J. G., Arango, M. I., & Zapata, G. (2020b). Riolitas del Alto Los Cacaos. In *Catálogos de las unidades litoestratigráficas de Colombia: Macizo de Santander*. Vol. 1. Servicio Geológico Colombiano. https://doi.org/10.32685/9789585279445.9

Daconte, R., & Salinas, R. (1980). *Geología de las planchas 66 Miraflores y 76 Ocaña. Departamento Norte de Santander. Memoria Explicativa. Escala 1:100.000*. Ingeominas.

Davidson, J., Turner, S., Handley, H., Macpherson, C., & Dosseto, A. (2007). Amphibole "sponge" in arc crust? *Geology*, 35, 787-790.

Dilles, J. H., Kent, A. J. R., Wooden, J. L., Tosdal, R. M., Koleszar, A., Lee, R. G., & Farmer, L. P. (2015). Zircon compositional evidence for sulfur-degassing from ore-forming arc magmas. *Economic Geology, 110*(1), 241-251. https://doi.org/10.2113/econgeo.110.1.241

Dörr, W., Grösser, J. R., Rodriguez, G. I., & Kramm, U. (1995). Zircon U-Pb age of the Paramo Rico tonalite-granodiorite, Santander Massif (cordillera Oriental, Colombia) and its geotectonic significance. *Journal of South American Earth Sciences, 8*(2), 187-194. https://doi.org/10.1016/0895-9811(95)00004-Y

Etayo Serna, F., Barrero, D., Lozano, H., Espinosa, A., González, H., Orrego, A., Ballesteros, I., Forero, H., Ramírez, C., Zambrano-Ortiz, F., Duque-Caro, H., Vargas, R., Núñez, A., Álvarez, J., Ropaín, C., Cardozo, E., Galvis, N., Sarmiento, L., Alberts, J. P. ... Hodges, C. A. (1985). *Mapa de terrenos geológicos de Colombia*. Ingeominas.

Gamboa Herrera, J. A. (2016). *Estudio de las alteraciones hidrotermales asociadas a sistemas de falla de dirección noreste en el Batolito de Mogotes (sector Mogotes-Alto de Los Cacaos: Macizo de Santander)* (Bachelor Thesis). Universidad Industrial de Santander.

Gardiner, N. J., Hawkesworth, C. J., Robb, L. J., Whitehouse, M. J., Roberts, N. M. W., Kirkland, C. L., & Evans, N. J. (2017). Contrasting granite metallogeny through the zircon record: A case study from Myanmar. *Scientific Reports, 7*(1), 1-8. https://doi.org/10.1038/s41598-017-00832-2

Goldsmith, R., Marvin, R. F., & Mehnert, H. H. (1971). *Radiometric ages in the Santander Massif, Eastern Cordillera, Colombian Andes*. Professional Paper 750-D, D44-D49. U. S. Geological Survey.

Guatame-García, L. A. (2009). *Caracterización de los depósitos hidrotermales con barita en cercanías al municipio de Hacarí, Norte de Santander* (Bachelor Thesis). Universidad Nacional de Colombia.

Hoskin, P. W. O., & Schaltegger, U. (2003). The composition of zircon and igneous and metamorphic petrogenesis. *Reviews in Mineralogy and Geochemistry, 53*(1), 27-62. https://doi.org/10.2113/0530027

Ishihara, S. (1978). Metallogenesis in the Japanese island arc system. *Journal of the Geological Society London*, 135, 389-406.

Ishihara, S. (1981). The granitoid series and mineralization. *Economic Geology Anniversary*, 75, 458-484.

Kammer, A. (1993). Steeply dipping basement faults and associated structures of the Santander Massif, Eastern Cordillera, Colombian Andes. *Geología Colombiana*, 18, 47-64.

Leal-Mejía, H. (2011). *Phanerozoic gold metallogeny in the Colombian Andes: A tectono-magmatic approach* (Ph. D. Thesis). Universitat de Barcelona.

Leal-Mejía, H., Shaw, R. P., & Melgarejo, J. C. (2019). Spatial-temporal migration of granitoid magmatism and the Phanerozoic tectono-magmatic evolution of the Colombian Andes. In F. Cediel, & R. P. Shaw (eds.), *Geology and tectonics of Northwestern South America* (pp. 253-410). Springer. https://doi.org/10.1007/978-3-319-76132-9_5

Loader, M. A., Wilkinson, J. J., & Armstrong, R. N. (2017). The effect of titanite crystallisation on Eu and Ce anomalies in zircon and its implications for the assessment of porphyry Cu deposit fertility. *Earth and Planetary Science Letters*, 472, 107-119. https://doi.org/10.1016/J.EPSL.2017.05.010

López-Isaza, J. A., & Zuluaga, C. A. (2020). Late Triassic to Jurassic magmatism in Colombia: Implications for the evolution of the northern margin of South America. In J. Gómez, & A. O. Pinilla-Pachón (eds.), *The geology of Colombia* (vol. 2, pp. 77-116). Servicio Geológico Colombiano. https://doi.org/10.32685/pub.esp.36.2019.03

Loucks, R. R. (2014). Distinctive composition of copper-ore-forming arcmagmas. *Australian Journal of Earth Sciences, 61*(1), 5-16. https://doi.org/10.1080/08120099.2013.865676

Lu, Y. J., Loucks, R. R., Fiorentini, M., Campbell Mccuaig, T., Evans, N. J., Yang, Z. M., Hou, Z. Q., Kirkland, C. L., Parra-Avila, L. A., & Kobussen, A. (2016). Zircon compositions as a pathfinder for porphyry Cu ±Mo±Au deposits. In J. P. Richards (ed.), *Tectonics and Metallogeny of the Tethyan Orogenic Belt* (pp. 329-347). Society of Economic Geologists. https://doi.org/10.5382/SP.19.13

Lu, Y., Evans, N., & Campbell McCuaig, T. (2019). *Zircon fingerprinting of magmatic-hydrothermal systems in the Archean Yilgarn Craton*. Report 197. Geological Survey of Western Australia. https://doi.org/10.13140/RG.2.2.26242.43201

Mantilla, L. C., & Mesa, A. (2002). Estudio geoquímico de elementos de tierras raras (REE) en las fluoritas de las minas Palestina (municipio de Cepita) y el Llantio (municipio de Los Santos) en el departamento de Santander: aporte al conocimiento del modelo genético. *Boletín de Geología*, *24*(39), 29-36.

Mantilla Figueroa, L. C., Bissig, T., Valencia, V., & Hart, C. J. R. (2013). The magmatic history of the Vetas-California mining district, Santander Massif, Eastern Cordillera, Colombia. *Journal of South American Earth Sciences*, 45, 235-249. https://doi.org/10.1016/j.jsames.2013.03.006

Mantilla Figueroa, L. C., García-Ramírez, C. A., & Valencia, V. A. (2016). Propuesta de escisión de la denominada "Formación Silgará" (Macizo de Santander, Colombia), a partir de edades U-Pb en circones detríticos. *Boletín de Geología, 38*(1), 33-50. https://doi.org/10.18273/REVBOL.V38N1-2016002

Mantilla Figueroa, L. C., Bissig, T., Cottle, J. M., & Hart, C. J. R. (2012). Remains of early Ordovician mantle-derived magmatism in the Santander Massif (Colombian Eastern Cordillera). *Journal of South American Earth Sciences*, 38, 1-12. https://doi.org/10.1016/j.jsames.2012.03.001

Mantilla Figueroa, L., Quintero, C., García, C., & Bartels. (2001). Estudio de los fluidos hidrotermales asociados a las mineralizaciones de fluorita. Sector Cepitá-Pescadero, Macizo de Santander. *Boletín de Geología*, *23*(38), 61-67.

Mojica, J., Kammer, A., & Ujueta, G. (1996). El Jurásico del sector noroccidental de Suramérica y guía de la excursión al valle superior del Magdalena (nov. 1-4/95), regiones de Payandé y Prado, departamento del Tolima. *Geología Colombiana*, 21, 3-40.

Ordóñez-Carmona, O. (2001). *Caracterização isotópica Rb-Sr e Sm-Nd dos principais eventos magmáticos nos Andes colombianos* (Ph. D. Thesis). Universidade de Brasilia.

Prieto D., Leal-Mejía H., López, J. A., Velásquez L., Sepúlveda M. J., Luengas C., Celada C., García D., Gómez M., Prieto, G., Peña, L. G., & Camacho, A. (2019). Mineralizaciones de metales base en la cordillera Oriental y el Macizo de Santander. Proyecto Mapa metalogénico de Colombia. In *XVII Congreso Colombiano de Geología. IV Simposio de Exploradores. Geología en tierra de Paz* (pp. 245-247). Sociedad Colombiana de Geología.

Restrepo-Pace, P. (1995). *Late Precambrian to early Mesozoic tectonic evolution of the Colombian Andes, based on new geochronological, geochemical and isotopic data* (Ph. D. Thesis). The University of Arizona.

Restrepo-Pace, P., Ruiz, J., Gehrels, G., & Cosca, M. (1997). Geochronology and Nd isotopic data of the Grenville-age rocks in the Colombian Andes: New constraints for Late Proterozoic-Early Paleozoic paleocontinental reconstructions of the Americas. *Earth and Planetary Science Letters, 150*(3-4), 427-441. https://doi.org/10.1016/S0012-821X(97)00091-5

Richards, J. P. (2015). The oxidation state, and sulfur and Cu contents of arc magmas: Implications for metallogeny. *Lithos*, 233, 27-45. https://doi.org/10.1016/J.LITHOS.2014.12.011

Richards, J., Spell, T., Rameh, E., Razique, A., & Fletcher, T. (2012). High Sr/Y magmas reflect arc maturity, high magmatic water content, and porphyry Cu±Mo±Au potential: Examples from the Tethyan arcs of central and eastern Iran and western Pakistan. *Economic Geology*, 107, 295-332.

Robb, L. J. (2005). *Introduction to ore-forming processes*. Blackwell Publishing.

Rodríguez, G. (2022). Petrographic, chemical and geochronological characteristics of the Onzaga Metarhyolite and its correlation with Ordovician magmatic events in the northern Andes, Colombia. *Boletín Geológico, 49*(1), 7-27. https://doi.org/10.32685/0120-1425/bol.geol.49.1.2022.571

Rodríguez, G., Zapata, G., Correa-Martínez, A. M., & Arango M. (2017). *Caracterización del magmatismo triásico-jurásico del Macizo de Santander*. Servicio Geológico Colombiano.

Rodríguez-García, G., Correa-Martínez, A. M., Zapata-García, G., Arango-Mejía, M. I., Obando-Erazo, G., Zapata-Villada, J. P., & Bermúdez, J. G. (2020a). Diverse Jurassic magmatic arcs of the Colombian Andes: Constraints from petrography, geochronology, and geochemistry. In J. Gómez, & A. O. Pinilla-Pachón (eds.), *The geology of Colombia*. Vol. 2. Servicio Geológico Colombiano. https://doi.org/10.32685/pub.esp.36.2019.04

Rodríguez, G., Correa Martínez, A. M., Arango, M. I., Zapata, G., & Bermúdez, J. G. (2020b). *Catálogos de las unidades litoestratigráficas de Colombia: Macizo de Santander*. Vol. 1. Servicio Geológico Colombiano. https://doi.org/10.32685/9789585279445

Rodríguez, G., Zapata, G., Arango, M. I., & Correa Martínez, A. M. (2020c). Monzogranito de Santa Bárbara. In *Catálogos de las unidades litoestratigráficas de Colombia: Macizo de San-*

tander. Vol. 1. Servicio Geológico Colombiano. https://doi.org/10.32685/9789585279445.3

Rodríguez, G., Correa Martínez, A. M., Zapata, G., & Arango, M. I. (2020d). Monzogranito de La Corcova. In *Catálogos de las unidades litoestratigráficas de Colombia: Macizo de Santander.* Vol. 1. Servicio Geológico Colombiano. https://doi.org/10.32685/9789585279445.4

Rodríguez, G., Zapata, G., Correa Martínez, A. M., & Arango, M. I. (2020e). Tonalita de San Martín. In *Catálogos de las unidades litoestratigráficas de Colombia: Macizo de Santander*. Vol. 1. Servicio Geológico Colombiano. https://doi.org/10.32685/9789585279445.6

Rodríguez, G., Arango, M. I., Correa Martínez, A. M., & Zapata, G. (2020f). Riolita de San Joaquín. In *Catálogos de las unidades litoestratigráficas de Colombia: Macizo de Santander*. Vol. 1. Servicio Geológico Colombiano. https://doi.org/10.32685/9789585279445.8

Rohrlach, B. D., & Loucks, R. R. (2005). Multi-million-year cyclic ramp-up of volatiles in a lower crustal magma reservoir trapped below the Tampakan copper-gold deposit by Mio-Pliocene crustal compression in the Southern Philippines. In T. M. Porter (ed.), *Super porphyry copper and gold deposits. A global perspective* (vol. 2, pp. 369-407). PGC Publishing.

Shen, P., Hattori, K., Pan, H., Jackson, S., & Seitmuratova, E. (2015). Oxidation condition and metal fertility of granitic magmas: Zircon trace-element data from porphyry Cu deposits in the Central Asian Orogenic Belt. *Economic Geology, 110*(7), 1861-1878. https://doi.org/10.2113/ECONGEO.110.7.1861

Sillitoe, R. H. (2010). Porphyry copper systems. *Economic Geology, 105*(1), 3-41. https://doi.org/10.2113/GSECONGEO.105.1.3

Spikings, R., Cochrane, R., Villagómez, D., Van der Lelij, R., Vallejo, C., Winkler, W., & Beate, B. (2015). The geological history of northwestern South America: From Pangaea to the early collision of the Caribbean Large Igneous Province (290-75 Ma). *Gondwana Research, 27*(1), 95-139. https://doi.org/10.1016/j.gr.2014.06.004

Sun, S., & McDonough, W. F. (1989). Chemical and isotopic systematics of ocean basalts: Implications for mantle composition and processes. *Geological Society, London, Special Publications, 42*(1), 313-345. https://doi.org/10.1144/GSL.SP.1989.042.01.19

Thompson, J. F. H., Sillitoe, R. H., Baker, T., Lang, J. R., & Mortensen, J. K. (1999). Intrusion-related gold deposits associated with tungsten-tin provinces. *Mineralium Deposita, 34*(4), 323-334. https://doi.org/10.1007/S001260050207

Trail, D., Bruce Watson, E., & Tailby, N. D. (2012). Ce and Eu anomalies in zircon as proxies for the oxidation state of magmas. *Geochimica et Cosmochimica Acta*, 97, 70-87. https://doi.org/10.1016/J.GCA.2012.08.032

Van der Lelij, R., Spikings, R., Ulianov, A., Chiaradia, M., & Mora, A. (2016). Palaeozoic to Early Jurassic history of the northwestern corner of Gondwana, and implications for the evolution of the Iapetus, Rheic and Pacific Oceans. *Gondwana Research*, 31, 271-294. https://doi.org/10.1016/J.GR.2015.01.011

Van der Lelij, R., Spikings, R., Gerdes, A., Chiaradia, M., Vennemann, T., & Mora, A. (2019). Multi-proxy isotopic tracing of magmatic sources and crustal recycling in the Palaeozoic to Early Jurassic active margin of North-Western Gondwana. *Gondwana Research, 66*, 227-245. https://doi.org/10.1016/j.gr.2018.09.007

Ward, D. E., Goldsmith, R., Cruz, J., & Restrepo, H. P. (1973). Geología de los cuadrángulos H-12 Bucaramanga y H-13 Pamplona, departamento de Santander. *Boletín Geológico, 21*(1-3), 132. https://doi.org/10.32685/0120-1425/bolgeol21.1-3.1973.383

Whitney, D. L., & Evans, B. W. (2010). Abbreviations for names of rock-forming minerals. *American Mineralogist, 95*(1), 185-187. https://doi.org/10.2138/AM.2010.3371

Willms, J. (1990). Barita y fluorita en la Mesa de Los Santos y Pescadero, Santander. *Boletín Geológico, 31*(2-3), 5-18. https://doi.org/10.32685/0120-1425/bolgeol31.2-3.1990.159

Zhong, S., Feng, C., Seltmann, R., Li, D., & Dai, Z. (2018). Geochemical contrasts between Late Triassic ore-bearing and barren intrusions in the Weibao Cu–Pb–Zn deposit, East Kunlun Mountains, NW China: Constraints from accessory minerals (zircon and apatite). *Mineralium Deposita, 53*(6), 855-870. https://doi.org/10.1007/S00126-017-0787-8

Zuluaga, C. A., & López, J. A. (2019). Ordovician Orogeny and Jurassic Low-Lying Orogen in the Santander Massif, Northern Andes (Colombia). In F. Cediel, & R. P. Shaw (eds.), *Geology and tectonics of Northwestern South America. Frontiers in Earth Sciences* (pp. 195-250). Springer. https://doi.org/10.1007/978-3-319-76132-9_4